

Article

Chemical Characteristics of Zircon from Khaldzan Burgedei Peralkaline Complex, Western Mongolia

Nergui Sarangua ^{1,*}, Yasushi Watanabe ¹, Takuya Echigo ¹ and Mihoko Hoshino ²

¹ Graduate school of International Resource Sciences, Akita University, Akita 010-0852, Japan; y-watanabe@gipc.akita-u.ac.jp (Y.W.); echigo@gipc.akita-u.ac.jp (T.E.)

² Institute for Geo-Resources and Environment, National Institute of Advanced Industrial Science and Technology, Tsukuba 350-0046, Japan; hoshino-m@aist.go.jp

* Correspondence: sarangua.nergui@gmail.com; Tel.: +81-80-5222-9869

Received: 5 October 2018; Accepted: 21 December 2018; Published: 24 December 2018



Abstract: The Khaldzan Burgedei peralkaline complex is one of the potential rare metal (Zr–Nb–REE) deposits in Mongolia. The complex consists mainly of quartz syenite and granite, and zircon is the most common accessory mineral in the rocks. Based on texture and mineral paragenesis, zircon is classified into three types. Type-I zircons in the quartz syenite and granite are generally isolated and euhedral to subhedral, 25–100 μm in size, enclosed by albite, K-feldspar, and quartz. Type-II zircons occur as subhedral to euhedral 20–150 μm grains, with quartz, and fluorite in the metasomatized zone in the quartz syenite as well as an upper part of the granite near the contact with the quartz syenite. These zircons contain porous core parts (Type-I) or remnants of corroded xenotime-(Y) and synchysite-(Ce). Type-III zircons are observed in the hydrothermally altered zone in quartz syenite and pegmatite. These zircons are anhedral, fine-grained, 10–30 μm in size, and occur in amphibole pseudomorphs which were replaced by quartz, fluorite, chlorite, and hematite. Laser Raman spectra show that Type-I and Type-II zircons contain high amounts of water. Among these, three types of zircons, Type-II zircons are most enriched in REE, Nb, and Th. The texture and composition of the three types of zircons indicate that Type-I, Type-II, and Type-III zircons are magmatic, metasomatic and late hydrothermal in origin, respectively, and they experienced remobilization and recrystallization during the transition from a magmatic to a hydrothermal system.

Keywords: zircon; metasomatism; Zr–Nb–REE mineralization; A-type granite; Khaldzan Burgedei

1. Introduction

A-type peralkaline granitic rocks are characterized by high FeO/MgO, K₂O/Na₂O ratio, low CaO, Al₂O₃ and H₂O, high concentration of high field strength elements (HFSE) and rare earth elements (REE) [1]. High concentrations of HFSE and REE in peralkaline granitic rocks have been reported from many igneous complexes such as Strange Lake, Canada [2], Bokan Mountain, USA [3], Midian Mountains, Saudi Arabia [4], and Khaldzan Burgedei, Mongolia [5] etc. In these igneous complexes, HFSE and REE mineralization have been considered to be formed by magmatic fractionation [2,5–7], metasomatic alteration, low temperature external hydrothermal fluids involvement [8], and/or a mixture of these processes [2,9–11].

The Khaldzan Burgedei complex in western Mongolia is 30 km long, up to 7 km wide, and is elongated in the N–S direction and subdivided two parts (Figure 1). The southern part is Khaldzan Burgedei, and the northern part is named the Tsahir Zr–Nb–REE group occurrence. The representative Khaldzan Burgedei REE deposit related to peralkaline granite and syenite is enriched in Zr, Nb, and REE [5].

In this complex, a variety of zirconium silicate minerals have been identified by previous researchers [5,10]. Based on the melt inclusion geochemistry, Kovalenko et al. [5] discussed the HFSE enrichment in the complex being due mainly to the fractionation of granitic magma. Kempe [10], in contrast, argued that the HFSE mineralization was due to magmatic and subsequent hydrothermal processes, later of which contributed to the enrichment of these elements significantly. They defined elpidite, gittinsite, and zircon by electron probe micro analyzer (EPMA) and scanning electron microscopy with energy dispersive X-ray (SEM-EDX). Although Kovalenko et al. [5] described how elpidite is the most common zirconium silicate mineral at Khaldzan Burgedei, Kempe et al. [9,10] clarified that zircon is the dominant phase in the complex. Kempe et al. [10] described that magmatic zircons are overgrown by hydrothermal zircons and suggested that zirconium silicates including zircons are a potential host of HREE based on the positive correlation between Zr and REE concentration in the rocks. In this study, we focused on zircon occurrence and chemistry to understand the enrichment process of HFSE and REE in the complex.

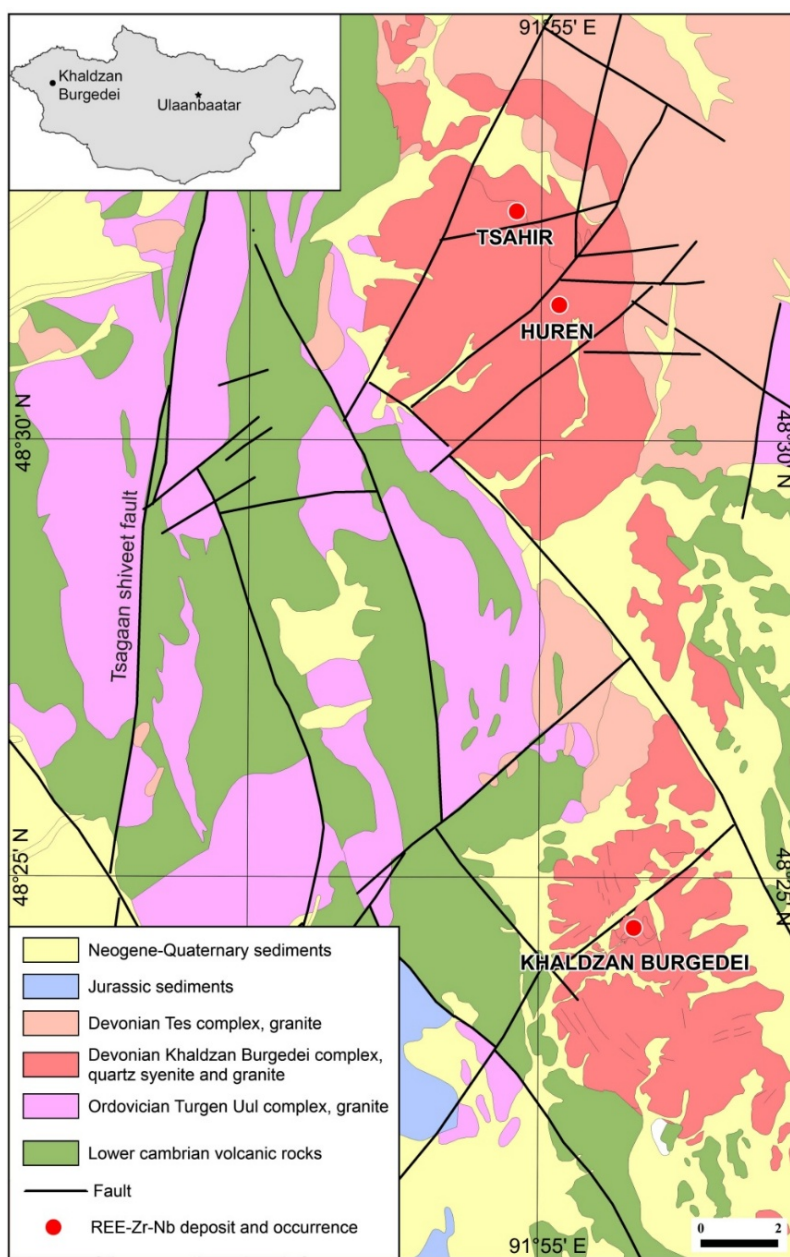


Figure 1. Regional geological map, modified from Miranov et al. [12].

2. Geology of the Khaldzan Burgedei Complex

The Devonian (380–400 Ma) Khaldzan Burgedei peralkaline complex is located in the N–S trending Paleozoic-Mesozoic rift zone in Western Mongolia [11,13]. It is located about 45 km northeast from the center of Khovd town.

The complex is oval-shaped, 7 km long and 5 km wide in size, and is elongated from the southeast–northwest direction. Geology around the complex consists of Vendian to Lower Cambrian sedimentary rocks and Ordovician biotite-amphibole granite (Figure 2a). The complex has multiple intrusive phases which are subdivided into eight phases [5]. HFSE and REE mineralization is associated with the metasomatized quartz syenite and granite [5]. The study area covers a western part of these mineralized bodies where Mongolian Lantanoide Corporation conducted exploration work in 2011 [14] (Figure 2b).

On the surface, quartz syenite occupies a major part of the complex (90%) (Figure 2a). The contact relation between quartz syenite and granite is either a sharp contact or intercalation of a 2–5.5 m thick transition zone, which consists of compositionally and texturally inhomogeneous rocks of syenite and pegmatite. The rock exhibits a miarolitic texture filled with pegmatitic amphibole, feldspar, and quartz. The quartz syenite is heavily metasomatized near the boundary of granite (Figure 2b).

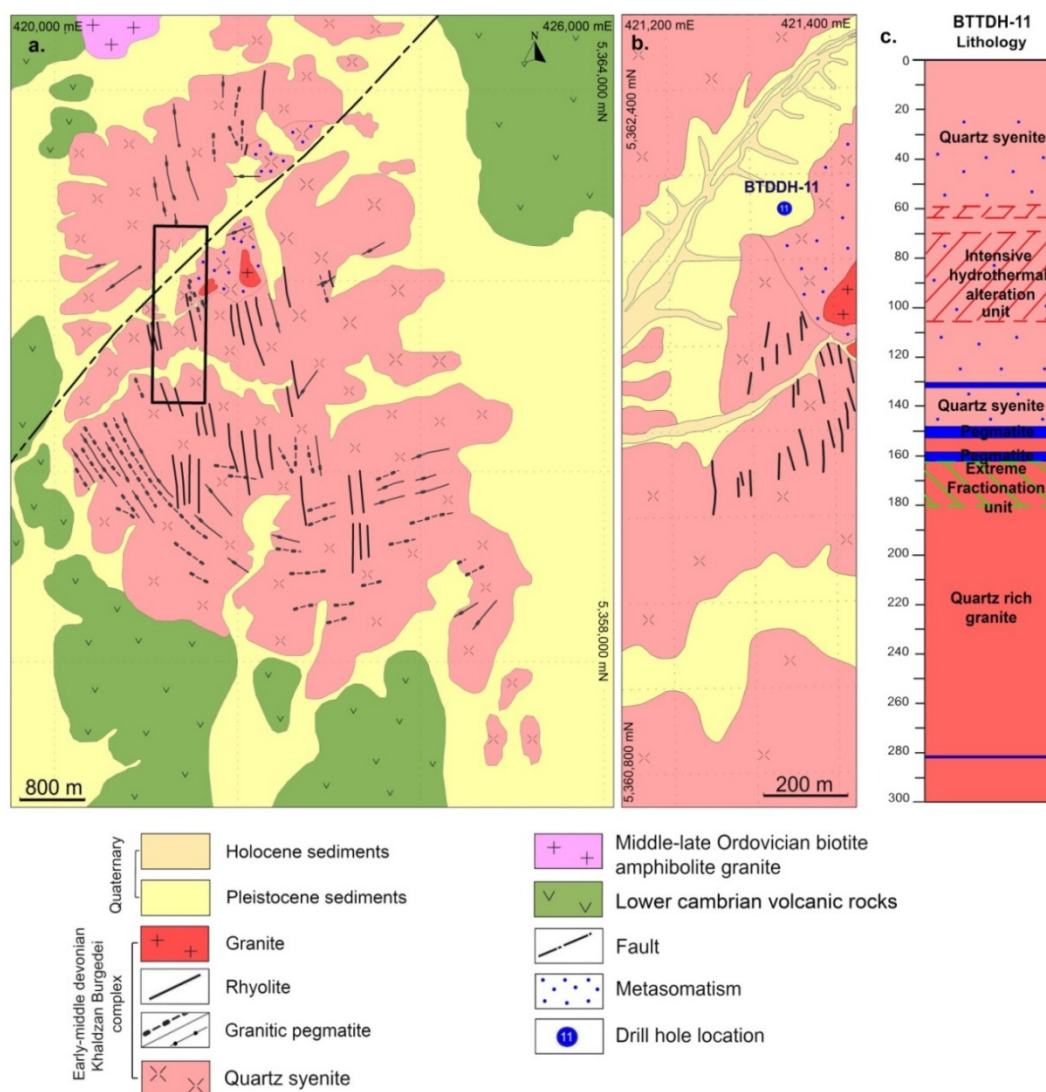


Figure 2. (a) Geological map of the Khaldzan Burgedei complex, modified from Kovalenko et al. [5], (b) Detailed map of the study area, and (c) BTDDH-11 drill hole core section.

3. Analytical Methods

Reconnaissance investigation of the whole complex was conducted to confirm the relationships between the intrusive rocks of the different units by surface geological mapping (Figure 2b). We also observed one of the cores drilled by the Mongolian Lantanoide Corporation in 2011 [14]. The samples used in this study are the drill hole: BTDDH-11 (8.4–293.4 m) (Figure 2c). Chemical composition of a total of 244 samples collected from this drill hole was determined by X-ray fluorescence (XRF) and Inductively coupled plasma mass spectrometry (ICP-MS). The samples were basically collected from one meter core intervals. These samples were crushed and pulverized to conduct whole-rock major and trace element analysis. The X-ray diffraction (XRD) and ICP-MS analyses were conducted at the Geological Survey of Japan (AIST), and the Activation Laboratory, Canada, respectively.

Petrographic and mineralogical studies were conducted for 22 polished thin sections with an optical microscope, and major and associated minerals were identified by a JEOL scanning electron microscope JSM-6610LV at Akita University. Analytical conditions were; accelerating voltage of 15 kV beam current 20 nA, beam diameter 5–10 μm and counting times 100 s.

The chemical composition of zircon grains was determined by a JEOL JXA-8530F electron probe microanalyzer (EMPA) at the Geological Survey of Japan, AIST. Elements detected with qualitative analysis were measured quantitatively with an acceleration voltage of 20 kV, a beam diameter of 5 μm and counting times of 20 s. The following peak position has been selected: the K series of X-ray spectra were used for Si, Al, Fe, Ca, Mn, Ti, P, and Na; the L series for Zr, REE, Hf, and Nb; the M series for Th and U. The following standards were used: Si–SiO₂, Zr–ZrO₂, Hf-metallic Hf, Y–Y₃Al₅O₁₂, Al–Al₂O₃, Fe–Fe₂O₃, Ca–CaSiO₃, Ti–TiO₂, Mn–MnO, Yb–YbP₅O₁₄, Dy–DyP₅O₁₄, Ce–CeB₆, P-monazite, Sn-cassiterite, Ho–HoP₅O₁₄, Er–ErP₅O₁₄, Gd–GdP₅O₁₄, U–UO₂, Th-monazite, Na–NaAlSi₃O₈, and Nd–NdAlO₃. All data were corrected with atomic number, absorption and characteristic fluorescence (ZAF) matrix-correction program. The structural formulae of the zircon grains were calculated on the basis of four oxygen atoms.

Laser Raman spectra of zircon were collected using a Renishaw RM200 Laser Raman Spectroscopy at Akita University. The laser beam diameter was 0.1 μm , and the collecting time was 10 s.

4. Results

4.1. Petrography and Geochemistry

The results of the geological mapping, core logging, and petrographic study with modal analysis show two igneous units in the studied area; quartz syenite and granite (Figure 2b,c and Figure 3). The occurrence of chilled margin in the granite at the contact with the quartz syenite indicates that the quartz syenite is earlier than the granite in the intrusive phase. The drill hole BTDDH-11 core consists of quartz syenite in the upper part (0.0–147.0 m), underlain by a transitional zone (quartz syenite and granite shows a mingling characteristic) with pegmatites (147.0–162.0 m), and granite in the lower part (162.0–293.4 m) (Figure 2c).

The quartz syenite (Figure 4a–d) is medium-to coarse-grained, holocrystalline and equigranular in texture. The unaltered/or weak altered part (0.0–14.0 m) of the quartz syenite mainly consists of arfvedsonite, K-feldspar, albite and quartz with accessory apatite, zircon, monazite, rutile, and titanite. The quartz syenite is affected by alkali metasomatism at the interval of 14.0–147.0 m. In this interval, feldspars are partly or completely replaced by albite. Most of the arfvedsonite is decomposed and replaced by fibrous aegirine and hematite, with interstitial fluorite, zircon, ilmenite, and quartz. In addition to this albitization, some parts of the rocks (58.0–106.0 m) are hydrothermally altered and fractured with chamosite, nontronite, calcite, hematite, fluorite with fluorite-quartz veinlets. These metasomatized and hydrothermally altered parts are enriched in HFSE and REE minerals, such as zircon, fersmite, pyrochlore, synchysite, bastnäsite, parasite, and xenotime.

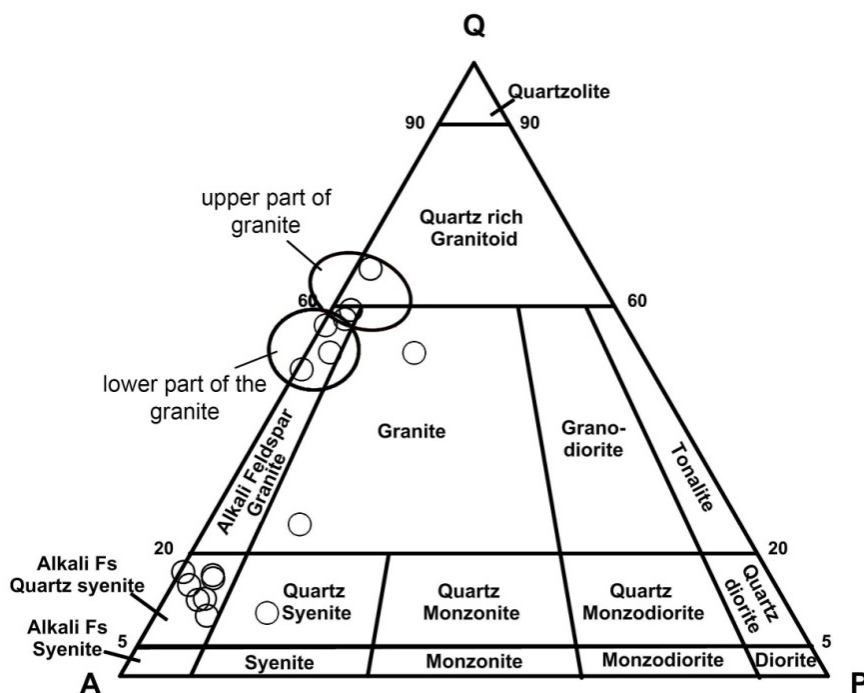


Figure 3. Quartz, alkali feldspar and plagioclase (QAP) diagram (Streickeisen, 1974) showing mineral modal abundance of the syenite and granite of the Khaldzan Burgedei complex.

The granite (Figure 4e,f) is fine to medium-grained, pinkish-grey, or yellowish-brown in color with rounded quartz, arfvedsonite, albite, and K-feldspar, and with accessory zircon, pyrochlore, and fluorite. Arfvedsonite, up to 0.5 cm, darkish-green and green in color, subhedral to anhedral in shape, shows twinning and its marginal parts are replaced by aegirine and hematite. Feldspars are subhedral to anhedral and late-stage fluorite, and quartz veinlets cut some feldspar phenocrysts. Quartz occurs interstitially to feldspars. The upper part of the granite, the interval between 162.0–180.0 m in the drill hole becomes quartz rich compared to the lower part (Figure 3).

Pegmatite (Figure 4g–j) occurs as veins, miarolitic cavity fillings, or irregular shaped pods in width of several tens cm. They are found particularly near the boundary between granite and quartz syenite. The pegmatite is composed of quartz, K-feldspar, albite with fine arfvedsonite, and with accessory zircon and fersmite.

The relation between quartz syenite and granite is clearly shown by field evidence, and together with the mineralogy and bulk chemistry of these rocks, it is suggested that the peralkaline magma evolved from quartz syenite to granite with time. The general compositional characteristics of quartz syenite and granite in the Khaldzan Burgedei complex show (Table A1) total REEs (1419–1641 ppm), Y (266–316 ppm), Zr (1548–1850 ppm) and Nb (272–401 ppm) in the quartz syenite. The granite has total REEs (881–2990 ppm), Y (294–418 ppm), Zr (2893–3639 ppm) and Nb (292–410 ppm) concentrations. The upper part of the granite unit (162.0–180.0 m) is enriched in quartz (Figure 3) and high in SiO₂ (71.5–79.3 wt %), and is depleted in other major elements (Al, Na, K). The highest total REE (1679.0–2991.1 ppm) concentrations occur in the upper part of the granite. Based on bulk rock compositions of the drill cores, an intense hydrothermal alteration unit within 58.0–106.0 m is enriched by Nb, Zr, Y, Ca and Sr, and SiO₂ and Na₂O content depleted comparison to the host albitized quartz syenite. The hydrothermal alteration unit shows concentrations of total REE (1408–2837 ppm), Y (186–743 ppm), Zr (945–8651 ppm) and Nb (332–409 ppm). The pegmatite has total REE (1367–2515 ppm), Y (329–400 ppm) Zr (3431–4396 ppm) and Nb (344–555 ppm) concentrations.

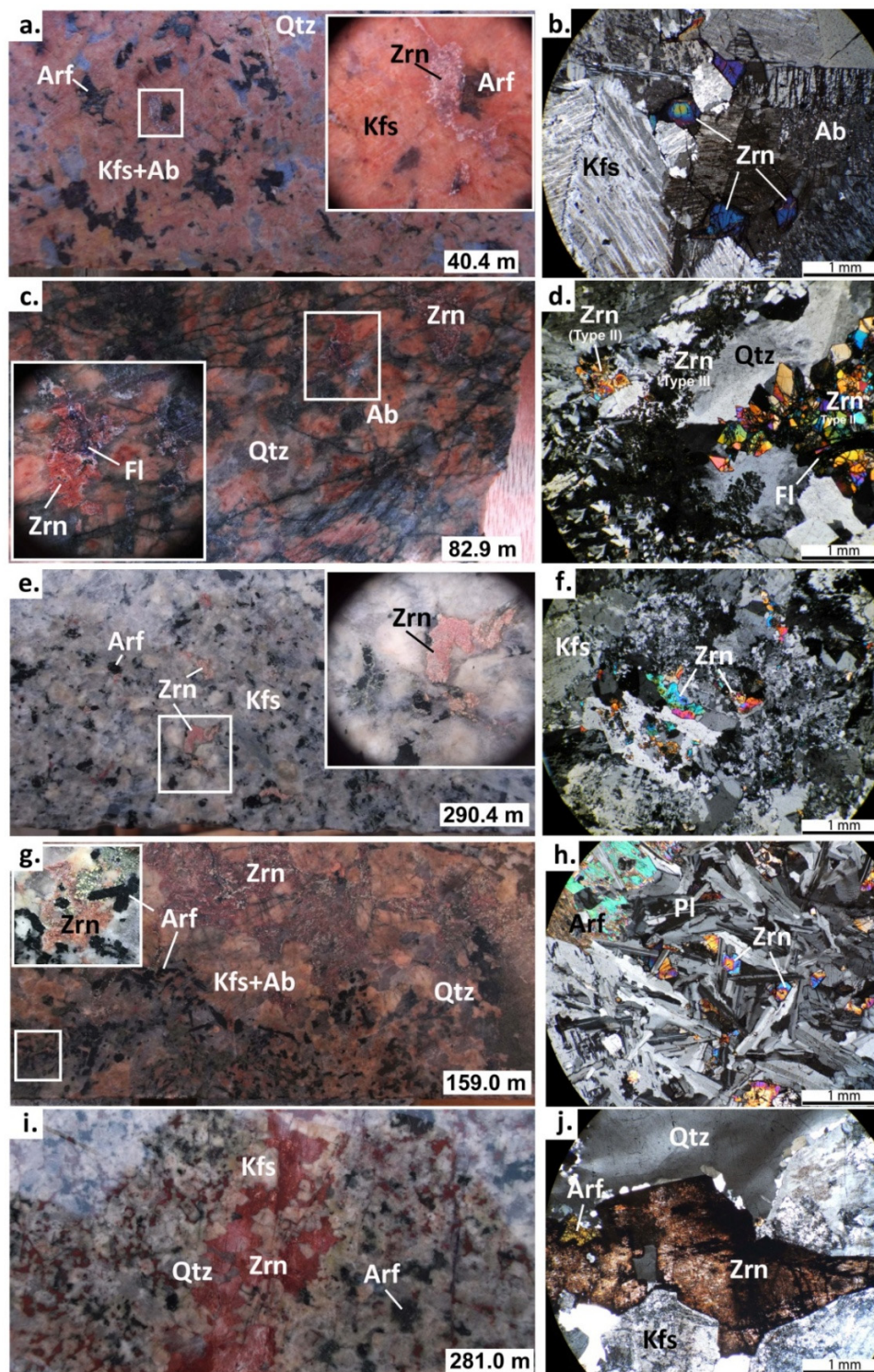


Figure 4. Rock units and photomicrographs. (a,b) quartz syenite; (a) coarse-grained quartz syenite that contains arfvedsonite, feldspars, and quartz with zircon, (b) feldspars with zircon (Type-I). (c,d) Metasomatized quartz syenite; (c) albitized quartz syenite that contains quartz, zircon and fluorite, (d) euhedral and subhedral Type-II zircon and anhedral fine-grained Type-III zircon with quartz and fluorite. (e,f) Granite; (e) fine-grained granite containing arfvedsonite, feldspar, and quartz with Type-I zircon, (f) zircons disseminated in the granite. (g–j) Pegmatite; (g) pegmatite with fine amphibole, large feldspar, quartz. White-colored zircons disseminated, (h) zircons interstitial to albite, (i) 1 cm-thick pegmatite that contains brown-colored zircon, quartz, and feldspar, (j) Zircon with quartz and feldspar. Abbreviations: Ab, albite; Arf, arfvedsonite; Kfs, K-feldspar; Pl, plagioclase; Qtz, quartz; Zrn, zircon; Fl, fluorite.

4.2. Zircon

4.2.1. Occurrence

Zircon is the most common accessory mineral in the quartz syenite and granite in this drill hole. Based on the mineral paragenesis and texture, these zircons are classified into three types (Type-I, Type-II, and Type-III) and Type-I is subdivided into three sub-types.

Type-I zircon in the quartz syenite is generally isolated, and euhedral to subhedral in crystal form. They are 25–100 μm in size, enclosed by albite, K-feldspar, or quartz (Figures 4 and 5). The zircons hosted in feldspar (Ia) are earlier than those hosted in quartz (Ib). These zircons are commonly zoned, and metamict. Metamict zircon in the back scatter detector (BSE) image show darkish-grey, thin rim (Figure 5a–c). Type-I zircons in granite (Ic) are also hosted in albite or K-feldspar, and less commonly quartz. They are euhedral in shape, compact and homogenous, although some of them are porous. They are sometimes corroded from the rims and include thin quartz band(s) in their crystals in the granite (Figure 5d). This texture suggests that zircons crystallized when quartz was saturated in the granitic magma. In the Cathodoluminescence (CL) images, Type-I zircons show grey, darkish grey background and quartz, and albite shows a dark background (Figure 5c,f).

Type-II zircons are frequently observed in the quartz syenite and granite. They occur as subhedral to euhedral 20–150 μm size grains, with quartz, fluorite, and chlorite (Figures 4 and 5). Zircons of this type are abundant in the metasomatized zone in the quartz syenite and upper part of the granite near the contact with the transition zone. Type-II zircons commonly form aggregates. These zircons enclose porous core parts (Type-I), and/or remnants of corroded xenotime-(Y) and synchysite-(Ce). Porous, inclusion-rich zircons with dark BSE intensity usually occur in central parts of grains (Figure 5g,h). In spite of the absence of clear zoning in zircons under BSE images, these zircons may have weak sector zoning and/or exsolution lamella, bright in color. Some zircons in the quartz syenite, show two clear stages of formation, inner lighter euhedral porous zircon (Type-I) enclosed by outer darker euhedral zircons (Type-II) with a distinct crystal boundary. These rims are heterogeneous in brightness with an irregular brightness boundary. The CL images show dark and grey background, corresponding to higher, and lower trace element contents [15], respectively, determined by EPMA. In addition, the image shows a halo in surrounding minerals. Radiation damage of the minerals surrounding zircons is in some cases visible in thin sections and is especially conspicuous in quartz (Figure 5l).

Type-III zircons are observed in the heavily hydrothermally altered zone in quartz syenite and pegmatite with Type-II zircons. The zircons of this type are euhedral or anhedral, fine-grained, 10–30 μm in size and occur in amphibole pseudomorphs replaced by quartz with fluorite, chlorite and hematite in addition to zircon (Figure 5m–o). They are generally homogeneous, and some anhedral zircons have an envelope of synchysite-(Ce). The CL images show that these zircons have a dark to bright background.

4.2.2. Chemistry

Chemical compositions of the zircons analyzed are shown in Table A2 and Figure 6 and the averaged composition of each zircon type is shown in Table 1 and Figure 7. Among the 198 zircon data, two data of which the total exceeds 103 wt % were excluded from the consideration.

The analytical data shows that only 40 data have the total between 99.00 and 101.00 wt %, and the others have the totals less than 99.00 wt %. The data of which total is less than 95 wt % is generally rich in U and Th, as well as FeO, suggesting metamictization with hematite and/or goethite. Zircons with low Zr content mainly occur in the metasomatized quartz syenite. These zircons contain abundant impurities such as Ca, Nb, Th, Fe, and REEs. Zircon in the granite shown opposite characteristic (Figure 6).

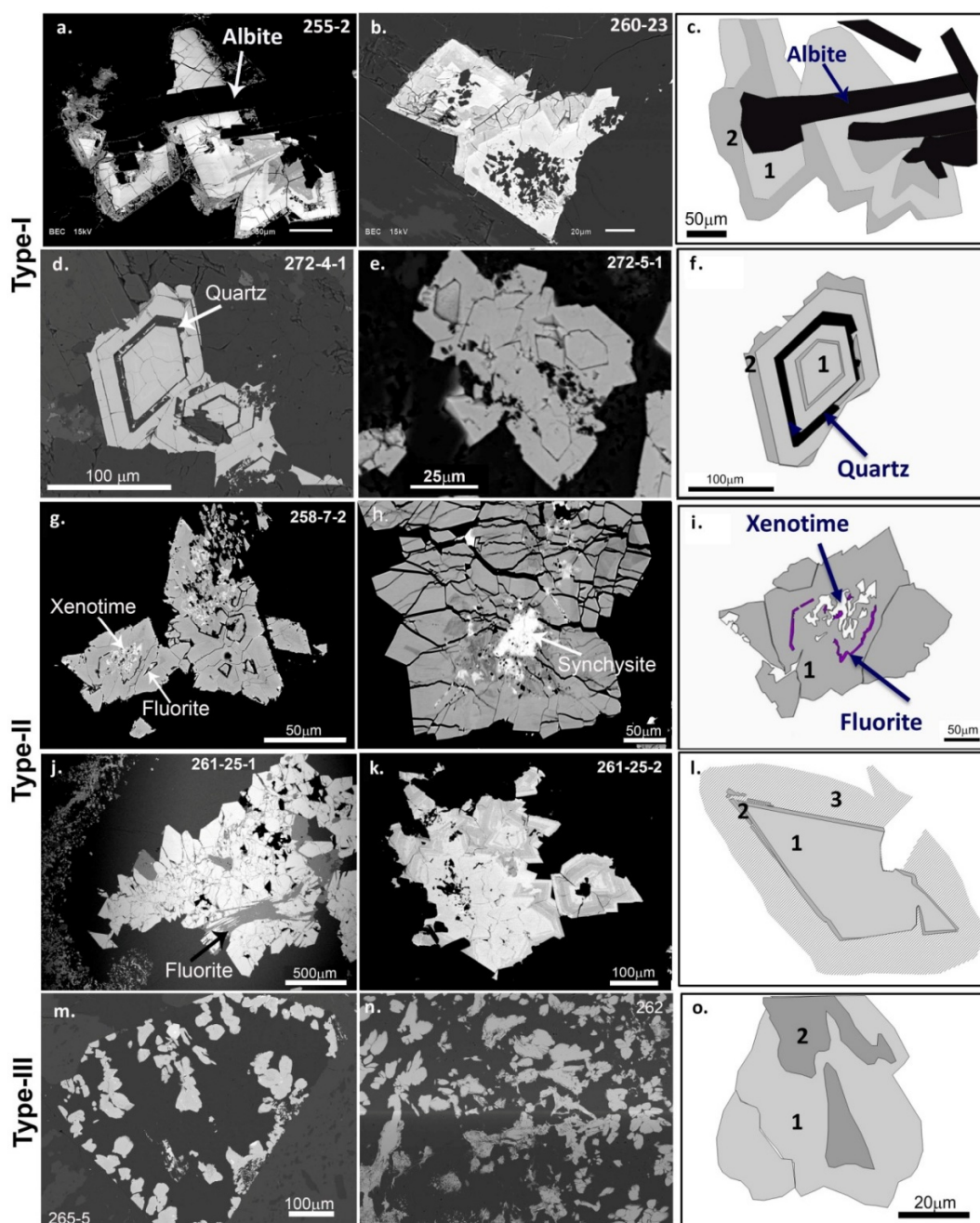


Figure 5. Zircon type and schematic drawings for cathodoluminescence images. (a,b) Type-Ia zircon from quartz syenite, zircon is show subhedral to euhedral shape, metamict zoning, and porous core. (c) Schematic drawing of Type-Ia zircons that consist of two domains, a bright CL domain 1, and grey CL domain 2. (d,e) Type-Ic zircon from granite. Zircon shows subhedral to euhedral shape and includes a thin quartz band. (f) Schematic drawing of Type-Ic zircons that consist of two domains, a grey CL domain 1, and bright CL domain 2. Two domains show zoning and contain dark quartz bands. (g,h), and (j,k) Type-II zircons from hydrothermal altered quartz syenite. These zircons show bright and dark color layered chemical zoning with porous cores. Xenotime and synchysite exist as inclusions in the zircon, (i) Schematic drawing of Type-II zircon. CL image shows dark grey solid domain 1, with white bright CL fluorite band (purple) and bright xenotime in the core, (l) Schematic drawing of Type-II zircon, with a grey CL euhedral core (domain 1), dark grey CL rim (domain 2) and whitish grey CL radiation halo in quartz (domain 3). Dark grey rim parts contain high Th concentration that attributed radiation halo. (m,n) Type-III zircons in the quartz syenite. Zircons are anhedral, fine-grained, and occur in an amphibole pseudomorph with quartz and fluorite. (o) Schematic drawing of Type-III zircons with anhedral grey and dark CL domains.

Variation for the Zr/Hf ratio is found: it is generally between 20 and 66, with most commonly average value at 46, suggesting significant fractionation between Zr and Hf (Figures 6 and 7). Increasing Hf concentration is assumed to reflect increasing degrees of differentiation [16]. Zr/Hf ratio values around 20 are found in the Type-III zircon, lower than chondrite Zr/Hf value is suggesting higher fractionation [17] and lower crystallization temperature [18]. The ratio between Si and Zr + Hf shows that Si dominates over Zr + Hf constantly. This suggests that Zr and Hf are substituted by other elements such as REE because a negative linear correlation between Zr + Hf and REE is observed.

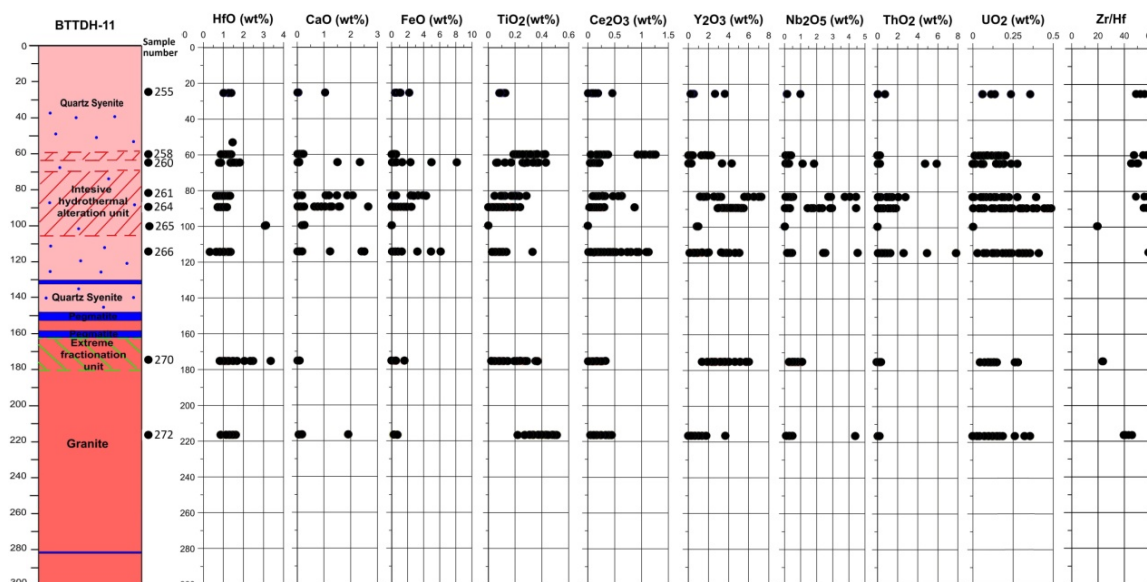


Figure 6. Zircon chemistry along the drill core BTDDH-11.

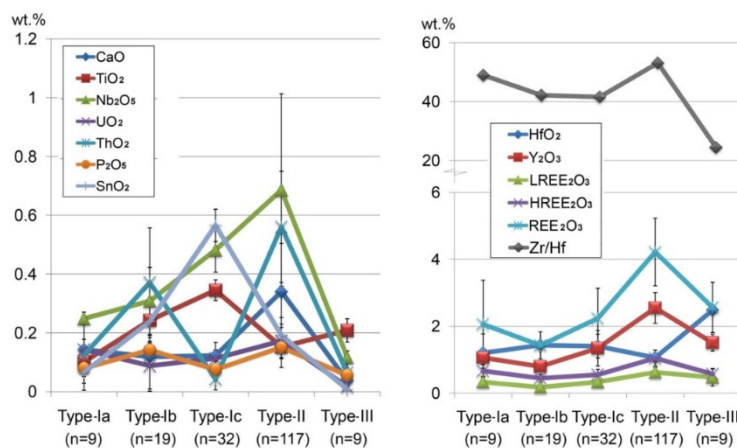


Figure 7. Zircon variation diagram.

The amounts of CaO is generally less than 0.3 wt % on average (Table 1 and Figure 7), although 25 analyzed points in zircons contain 0.5–2.6 wt % (Figure 5). Such Ca-rich zircons occur as dark rims or internal bands in zircon grains in the metasomatized and hydrothermally altered quartz syenite. Only one quartz syenite sample from the heavily altered zone contains zircons with appreciable amounts (0.43–0.58 wt %) of Na₂O.

Type-III and Type-II zircons are highest (99.26 wt %) and lowest (96.66 wt %) in the average of analytical totals among these three types (Table 1). The contents of SnO₂ and TiO₂ in zircon increase from Type-Ia to Type-Ic through Type-Ib, but they are lower in Type-II than in Type-Ib and Type-Ic. The Nb₂O₅ content also increases from Type-Ia to Type-Ic, and it is highest in Type-II. The content of CaO and UO₂ are similar in Type-Ia, Ib and Ic zircons, respectively, and they are higher in Type-II than

in Type-I zircons. Ca, Fe, Nb, and Th-rich zircons occur in the Type-II zircons in the metasomatized zone. ThO₂ and P₂O₅ contents are high in Type-Ib and Type-II, respectively. All these elements are lower in Type-III compared with Type-II, except TiO₂ (Figure 6). The total REE₂O₃ content in zircon is 2.50 wt % on average, and it is higher (4.22 wt %) in Type-II than Type-I (1.91 wt %) and Type-III (2.56 wt %). High-REE Type-II zircons mainly occur in the highly metasomatized part of the quartz syenite (Figure 6). The LREE/HREE ratio is 0.14 for Type-Ib, 0.18 for Type-Ic, 0.19 for Type-Ia, 0.17 for Type-II, and 0.22 for Type-III. In general, HREE is more enriched in the core parts than the rim parts in Type-I zircons, whereas it is opposite in Type-II zircons.

Table 1. Average value of electron probe micro analyzer (EPMA) analysis data in zircon.

Type	Type-Ia		Type-Ib		Type-Ic		Type-II		Type-III	
Comment	Average	std	Average	std	Average	std	Average	std	Average	std
n	9		19		32		117		9	
SiO ₂	32.58	(0.461)	33.46	(0.412)	32.07	(0.707)	31.28	(2.931)	32.85	(0.568)
ZrO ₂	59.78	(1.221)	62.17	(1.028)	58.58	(1.535)	57.22	(5.543)	60.27	(1.294)
HfO ₂	1.23	(0.113)	1.47	(0.192)	1.53	(0.563)	1.08	(0.200)	2.16	(1.082)
Al ₂ O ₃	0.15	(0.078)	0.09	(0.047)	0.17	(0.067)	0.15	(0.133)	0.20	(0.087)
CaO	0.03	(0.013)	0.04	(0.023)	0.07	(0.041)	0.32	(0.555)	0.15	(0.116)
TiO ₂	0.10	(0.016)	0.28	(0.086)	0.36	(0.155)	0.18	(0.124)	0.17	(0.055)
Y ₂ O ₃	0.86	(1.143)	0.06	(0.096)	1.24	(1.841)	2.48	(2.079)	1.58	(0.099)
Nb ₂ O ₅	0.16	(0.027)	0.20	(0.049)	0.33	(0.147)	0.65	(1.144)	0.51	(0.419)
Ce ₂ O ₃	0.18	(0.217)	0.10	(0.049)	0.15	(0.133)	0.31	(0.300)	0.59	(0.042)
Nd ₂ O ₃	0.07	(0.128)	0.00	(0.000)	0.04	(0.067)	0.14	(0.181)	0.21	(0.064)
Gd ₂ O ₃	0.05	(0.091)	0.02	(0.027)	0.16	(0.224)	0.18	(0.128)	0.10	(0.035)
Dy ₂ O ₃	0.24	(0.137)	0.17	(0.049)	0.32	(0.155)	0.49	(0.322)	0.19	(0.028)
Ho ₂ O ₃	0.02	(0.029)	0.03	(0.039)	0.04	(0.051)	0.08	(0.071)	0.09	(0.049)
Er ₂ O ₃	0.32	(0.147)	0.06	(0.048)	0.15	(0.142)	0.44	(0.358)	0.31	(0.028)
Yb ₂ O ₃	1.05	(0.321)	0.09	(0.161)	0.18	(0.221)	0.75	(0.596)	0.65	(0.035)
UO ₂	0.12	(0.077)	0.09	(0.092)	0.11	(0.079)	0.15	(0.115)	0.04	(0.049)
ThO ₂	0.14	(0.261)	0.06	(0.073)	0.06	(0.058)	0.34	(0.582)	0.07	(0.035)
FeO	0.84	(0.625)	0.70	(0.746)	0.41	(0.147)	0.64	(0.935)	0.15	(0.007)
P ₂ O ₅	0.07	(0.032)	0.04	(0.027)	0.08	(0.063)	0.15	(0.192)	0.05	(0.053)
SnO ₂	0.07	(0.075)	0.32	(0.124)	0.60	(0.313)	0.24	(0.234)	0.00	(0.000)
Total	98.06		99.46		96.62		97.27		97.89	
LREE ₂ O ₃	0.28	(0.349)	0.11	(0.054)	0.1847	(0.148)	0.6185	(0.487)	0.445	(0.514)
HREE ₂ O ₃	1.45	(1.363)	0.33	(0.127)	1.7456	(2.139)	3.4871	(2.772)	1.0825	(1.251)
REE ₂ O ₃	1.73	(1.613)	0.43	(0.139)	1.9303	(2.137)	4.1056	(2.882)	1.5275	(1.764)
Structural formulae based on 4 oxygen atoms										
Si	1.023	(0.011)	1.025	(0.006)	1.018	(0.012)	0.999	(0.049)	1.016	(0.011)
Zr	0.915	(0.014)	0.929	(0.009)	0.907	(0.015)	0.891	(0.045)	0.936	(0.034)
Hf	0.011	(0.001)	0.013	(0.002)	0.014	(0.005)	0.010	(0.001)	0.011	(0.000)
Al	0.006	(0.003)	0.003	(0.002)	0.006	(0.003)	0.006	(0.006)	0.007	(0.003)
Ca	0.001	(0.000)	0.001	(0.001)	0.002	(0.001)	0.012	(0.022)	0.005	(0.004)
Ti	0.002	(0.000)	0.007	(0.002)	0.009	(0.004)	0.004	(0.003)	0.007	(0.003)
Y	0.015	(0.019)	0.001	(0.002)	0.021	(0.032)	0.044	(0.039)	0.026	(0.001)
Nb	0.002	(0.000)	0.003	(0.001)	0.005	(0.002)	0.010	(0.019)	0.008	(0.007)
Ce	0.002	(0.003)	0.001	(0.001)	0.002	(0.002)	0.004	(0.003)	0.007	(0.001)
Nd	0.001	(0.001)	0.000	(0.000)	0.000	(0.001)	0.002	(0.002)	0.003	(0.001)
Gd	0.000	(0.001)	0.000	(0.000)	0.002	(0.002)	0.002	(0.001)	0.001	(0.000)
Dy	0.002	(0.001)	0.002	(0.000)	0.003	(0.002)	0.005	(0.004)	0.002	(0.000)
Ho	0.000	(0.000)	0.000	(0.000)	0.000	(0.001)	0.001	(0.001)	0.001	(0.000)
Er	0.003	(0.001)	0.001	(0.000)	0.002	(0.001)	0.005	(0.004)	0.003	(0.000)
Yb	0.010	(0.003)	0.001	(0.001)	0.002	(0.002)	0.008	(0.006)	0.006	(0.000)
U	0.001	(0.001)	0.001	(0.002)	0.001	(0.001)	0.001	(0.001)	0.000	(0.000)
Th	0.001	(0.002)	0.000	(0.001)	0.000	(0.000)	0.003	(0.005)	0.001	(0.001)
Fe	0.022	(0.016)	0.018	(0.019)	0.011	(0.004)	0.018	(0.029)	0.002	(0.002)
P	0.002	(0.001)	0.001	(0.001)	0.002	(0.002)	0.004	(0.005)	0.003	(0.001)
Sn	0.001	(0.001)	0.004	(0.002)	0.007	(0.004)	0.003	(0.003)	0.000	(0.000)
Total	2.020		2.011		2.015		2.030		2.026	

4.2.3. Laser Raman Spectroscopy

Results of the Raman spectra show three type zircons have a damaging effect of radiation. Each Si–O peak in the spectra is shifted from the original position and molecular water peaks are detected (Figure 8).

The Raman spectra of Type-I zircons show high Raman intensity and wave number shifts. The bands of the Si–O asymmetric stretching vibration at 1008 cm^{-1} are observed at 1001 cm^{-1} and the bands of the Si–O symmetric bending vibration are observed at 437 cm^{-1} . The strong Raman bands observed at 2237 and 2525 cm^{-1} are attributed to a Th compound. The molecular water vibration bands are observed at 3390 and 3600 cm^{-1} .

As shown in the Raman spectra, Type-II zircons show high Raman intensity and broad peaks. The bands of SiO_4 are observed at 978 cm^{-1} and 779 cm^{-1} and the bands of the Si–O symmetric bending vibration is observed at 437 cm^{-1} . The Th broad bands are observed at 2428 to 2465 cm^{-1} . The molecular water broad peak is observed between 3300 to 3700 cm^{-1} .

The Raman spectra of Type-III zircons show low intensity, and SiO_4 peaks are observed at 432 and 995 cm^{-1} . The Th bands are observed at 2032 , 2233 and 2507 cm^{-1} . The spectra show very low molecular water vibration peaks at 3405 and 3614 cm^{-1} .

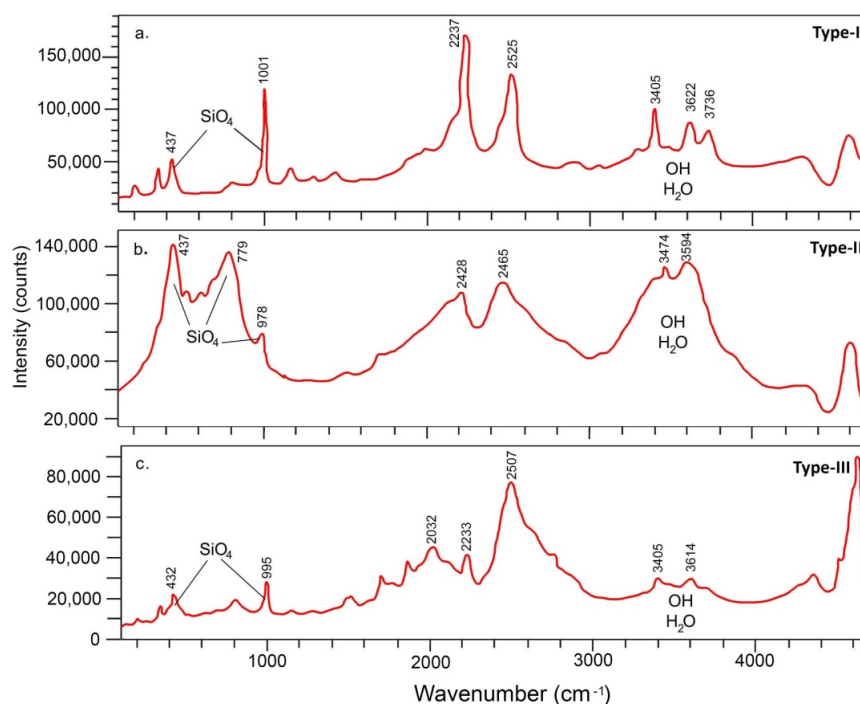


Figure 8. Result of laser Raman spectroscopy for different zircon types.

5. Discussion

Results of the zircon occurrence, mineral paragenesis, texture, and chemistry show that zircons formed at different stages (Type-I, II and III) have different characteristics as summarized in Table 2.

The Khaldzan Burgedei complex has the characteristics of peralkaline intrusive rocks, and the evolution of peralkaline magma formed quartz syenite and granite [5].

Type-I zircon is the primary accessory mineral in the quartz syenite and granite. Mineral paragenesis shows that zircon became saturated in the quartz syenite magma before quartz saturation, resulting in the precipitation of Type-Ia zircons. This saturation then continued until the end of the granite and pegmatite formation. During the fractionation of the magma from quartz syenite to granite, zircons became more enriched in HFSE (e.g., Nb, Th, and Sn) and this suggests that HFSE became concentrated in the fractionated granitic magma.

Table 2. Summary of the characteristics of zircon types.

Zircon Type	Zoning	Chemical Composition (Average Anomaly by EPMA)	Molecular Water (by Laser Raman)	Origin
Type-I	Banded zoning with quartz	Y ₂ O ₃ 1.35 wt % ΣREE ₂ O ₃ 2.24 wt % Nb ₂ O ₅ 0.48 wt %	3390 and 3600 cm ⁻¹ vibration peak	Magmatic
Type-II	Oscillatory zoning with porous core	Y ₂ O ₃ 2.55 wt % ΣREE ₂ O ₃ 4.22 wt % Nb ₂ O ₅ 0.69 wt %	3250–3700 cm ⁻¹ broad peak	Metasomatic
Type-III	Homogeneous	Y ₂ O ₃ 1.51 wt % ΣREE ₂ O ₃ 2.56 wt % Nb ₂ O ₅ 0.12 wt %	No peak	Late hydrothermal

The hydrothermal activity started by alkali metasomatism followed by lower temperature hydrothermal alteration. The porous occurrence of Type-I zircons suggest of fluorine and sodium rich hydrothermal fluids leached HREEs from Type-I zircons and transported the host quartz syenite. Type-II zircons typically occur in the metasomatized and hydrothermal parts of the quartz syenite and include corroded REE carbonates and phosphates. They also include porous Type-I zircons in the cores. This occurrence suggests that Type-II zircons formed during the metasomatism [15]. The high concentration of Nb, Th, U and P in Type-II zircons indicate that metasomatic fluids reacted with Type-I zircons and/or phosphate minerals and extracted minor elements such as Th, U, and P which reprecipitated in Type-II zircons, resulting in a high concentration of these elements. The intimate association of fluorite with Type-II zircons and a higher concentration of Ca in Type II zircons suggest that addition of Ca into the hydrothermal fluids may have destabilized a zirconium–fluorite complex in the fluids, resulting in the precipitation of zircon and fluorite [19]. The highest concentrations of hydration in Type-II zircon suggested by the Raman spectra data and low analytical totals (EPMA) also suggest a metasomatic origin for Type-II zircons [20].

Type-III zircons are latest and occur with fluorite and quartz. They formed in amphibole pseudomorphs. The pseudomorphs texture and mineral paragenesis is suggested this replacement reaction related to Ca–F bearing hydrothermal alteration. The low Zr/Hf ratios in the Type-III zircon suggest the fractionation of zirconium at a lower temperature [16,17]. Due to a low crystallization temperature, Type-II zircons have chemical compositions closer to the stoichiometry, and this may have resulted in intimate synchysite-(Ce) crystallization with Type-III zircons.

6. Conclusions

Observation on the texture and chemical composition of zircon provide unique insights into the various stages of magma differentiation. Three zircon types, magmatic (Type-I), metasomatic (Type-II), and late hydrothermal (Type-III), are recognized in the quartz syenite and granite of the Khaldzan Burgedei complex in Mongolia. These zircons record a magmatic evolution of the complex, such that there are HFSE enrichments in the fractionated peralkaline granite, and redistribution of the minor elements such as Th, U, and REE during the subsequent metasomatism and hydrothermal alteration. Metasomatic fluids reacted with Type-I zircons and extracted minor elements which reprecipitated in Type-II zircons, resulting in a high concentration of these elements. Zircons are a good indicator with which to trace the behavior of HFSE and REE in the peralkaline magmatic-hydrothermal system.

Author Contributions: Conceptualization, N.S., Y.W., and T.E.; Methodology, M.H.; T.E.; and N.S.; Investigation, Y.W., N.S. and T.E.; Writing-Original Draft Preparation, N.S.; Writing-Review and Editing, Y.W.; Visualization, Y.W.

Acknowledgments: We gratefully thank the Mongolian Lantanoide Corporation support in fieldwork and drill core observation. We would like to thank the staff of the National Institute of Advanced Industrial Science and Technology for Geological Survey of Japan, AIST, for their help in EPMA and SEM-EDX analyzes.

Conflicts of Interest: The authors declare no conflict of interest.

Appendix A

Table A1. Major and trace element data of representative Khaldzan Burgedei complex.

Lithology	Quartz Syenite			Metasomatized/Hyd. Altered Quartz Syenite				Granite			Fractionated Granite		Pegmatite	
Sample No	1721	1732	1737	1767	1796	1809	1839	1893	1904	1913	1861	1875	1856	1949
(wt %)														
SiO ₂	65.8	66.7	66.8	66.2	62.2	64.3	64.5	71.8	69.9	71.2	71.9	77.2	71.8	71.2
Al ₂ O ₃	13.6	12.7	13.7	13.9	14.0	12.9	10.9	10.1	9.3	11.3	11.6	6.6	10.4	11.6
Fe ₂ O ₃ (T)	4.6	6.9	6.0	5.5	4.8	6.4	8.7	5.0	5.9	4.5	3.4	6.3	5.5	4.5
MnO	0.1	0.1	0.1	0.2	0.1	0.2	0.2	0.1	0.2	0.1	0.1	0.1	0.1	0.1
MgO	0.0	0.01	0.0	0.0	0.0	0.1	0.0	0.0	<0.01	<0.01	0.0	<0.01	0.0	0.0
CaO	1.9	1.2	1.2	1.0	2.3	3.0	2.3	2.1	3.2	1.0	0.9	0.3	0.8	0.5
Na ₂ O	4.5	4.6	5.4	6.1	4.8	4.3	5.6	4.0	3.5	4.2	3.5	3.4	4.6	5.0
K ₂ O	5.3	5.6	5.2	5.1	5.1	4.5	3.8	4.3	4.1	4.8	5.6	2.8	4.2	4.2
TiO ₂	0.2	0.2	0.2	0.3	0.2	0.3	0.3	0.1	0.1	0.1	0.1	0.1	0.2	0.2
P ₂ O ₅	<0.01	0.0	<0.01	0.0	0.0	0.0	<0.01	<0.01	<0.01	<0.01	0.0	<0.01	0.0	0.0
LOI	1.9	1.3	1.3	1.1	3.6	3.6	1.6	1.1	1.6	1.2	1.2	0.6	0.6	0.7
Total	97.9	99.3	99.7	99.2	97.2	99.6	98.0	98.5	97.9	98.4	98.3	97.4	98.1	98.0
(ppm)														
Sc	<1	<1	<1	<1	<1	<1	<1	<1	<1	<1	<1	<1	<1	<1
Be	21	29	17	28	19	20	16	24	17	34	24	13	19	29
V	<5	<5	<5	<5	<5	<5	5	<5	<5	<5	<5	<5	<5	<5
Cr	<20	<20	<20	<20	<20	<20	<20	<20	<20	<20	<20	<20	<20	<20
Co	<1	<1	<1	32	18	<1	<1	<1	<1	<1	<1	<1	<1	<1
Ni	<20	<20	<20	<20	<20	<20	<20	<20	<20	<20	<20	<20	<20	<20
Cu	<10	<10	<10	<10	<10	10	<10	<10	<10	<10	<10	<10	30	<10
Ga	53	49	52	52	59	47	44	54	52	64	63	40	49	61
Ge	3	4	4	4	3	3	5	3	4	3	3	4	3	4
As	10	8	7	<5	<5	<5	<5	8	11	9	6	<5	11	27
Rb	290	301	283	251	271	197	205	283	302	366	477	250	262	274
Sr	41	53	37	35	32	80	104	126	209	67	49	23	41	30
Y	299	316	275	251	412	356	411	309	250	418	391	291	329	400
Zr	1850	1657	1548	2822	3482	2247	3279	2893	3639	2992	4479	3468	4396	3431
Nb	335	401	272	371	460	421	496	385	410	585	399	354	555	344
Mo	<2	<2	5	<2	3	6	<2	5	<2	<2	<2	<2	3	2
In	<0.2	<0.2	<0.2	<0.2	<0.2	<0.2	<0.2	<0.2	<0.2	<0.2	<0.2	<0.2	<0.2	<0.2
Sn	25	31	20	31	29	22	46	39	36	34	26	23	42	25
Sb	0.9	0.5	<0.5	<0.5	<0.5	0.5	<0.5	1.4	0.7	0.9	1.6	1	<0.5	0.8
Cs	0.6	0.5	0.7	<0.5	<0.5	<0.5	<0.5	0.7	1	0.9	0.9	0.7	1	0.8
Ba	43	31	29	44	55	46	54	42	32	39	27	26	60	55

Table A1. Cont.

Lithology	Quartz Syenite			Metasomatized/Hyd. Altered Quartz Syenite				Granite			Fractionated Granite		Pegmatite	
Sample No	1721	1732	1737	1767	1796	1809	1839	1893	1904	1913	1861	1875	1856	1949
Bi	<0.4	<0.4	<0.4	<0.4	<0.4	<0.4	<0.4	<0.4	<0.4	<0.4	0.8	0.7	0.4	0.6
La	343	389	344	486	632	471	271	221	156	226	603	670	276	532
Ce	556	643	561	802	1090	767	539	456	333	479	1090	1130	524	1010
Pr	68.9	78.1	66.4	92.6	116	85.6	66.9	56.5	40	57.8	120	133	63.6	120
Nd	256	284	241	316	394	291	263	215	151	222	451	504	242	469
Sm	50.2	54.3	46	53.1	72.8	50.7	56.7	49.5	36.2	54.2	79.9	83.4	52.6	95.8
Eu	3.59	3.61	2.92	3.27	4.84	3.35	3.49	3.02	1.75	3.32	4.57	4.6	3.47	5.59
Gd	47.3	52.3	44.8	48.8	67.2	44.7	52.1	48.7	33	52.4	68.9	70.8	51.2	84.9
Tb	8.2	9.3	7.4	7.7	12.2	8.5	9	9.1	6.4	10.6	10.9	9.2	9.5	12.5
Dy	48.6	53.8	42.9	44	73.6	52.4	54.6	54.7	40.9	69.9	66.7	50.2	57.9	71.8
Ho	9.6	10.3	8.5	8.5	14.4	10.8	11.3	10.7	9	14.8	13.6	10	11.5	14.1
Er	27.5	28.7	24.3	24.8	42.1	33.7	34.9	30.6	30.6	48.9	42.4	31.2	33.4	43.8
Tm	4.03	4.17	3.6	3.75	6.13	5.39	5.51	4.91	5.12	7.66	6.75	5.01	5.03	6.73
Yb	24.8	26.2	23	24.3	37.6	34.3	35.6	30	34	45.6	43.4	31.7	32.3	42.5
Lu	3.46	3.83	3.35	3.52	5.2	4.85	5.22	4.21	4.91	6.1	6.03	4.74	4.75	6.14
Hf	45.3	40.9	35.8	65.9	81.9	48	66.9	66.6	90.2	66.1	106	80.4	106	72.4
Ta	21.6	27.5	17.7	25.8	29.6	23.6	35.1	30	33.8	40.2	30.5	28.8	36.6	31.7
W	3	1	<1	324	196	1	<1	<1	<1	<1	<1	<1	<1	<1
Tl	0.4	0.5	0.5	0.4	0.3	0.2	0.1	0.4	<0.1	<0.1	0.5	0.3	0.6	0.5
Pb	10	67	42	60	15	42	54	26	27	87	34	52	81	65
Th	43.4	51	38.8	40.7	66.8	53.3	42.3	47.3	21.9	66.5	66.7	31.1	65.8	50
U	13.9	15.3	10.5	15.8	19.3	16.6	15.4	16.8	15.5	22.6	17.3	15.1	23	13.8
Zn	190	410	320	440	240	370	630	470	460	430	340	510	510	374

Table A2. EPMA analysis. Zircon in the Khaldzan Burgedei complex.

Type I													
Sample No	260			272-P4				272-P5			255-P2		
Comment	Core	Rim		Core	Rim		Core	Core		Rim			
n	7	std	3	std	5	std	4	std	6	std	3	std	1
SiO ₂	33.69	(0.06)	33.34	(0.44)	32.30	(0.22)	32.08	(0.41)	32.72	(0.11)	32.04	(0.39)	27.01
ZrO ₂	62.42	(0.23)	62.55	(1.41)	59.01	(0.47)	58.73	(0.61)	60.01	(0.39)	58.18	(1.22)	52.45
HfO ₂	1.56	(0.14)	1.46	(0.13)	1.44	(0.07)	1.35	(0.08)	1.34	(0.04)	1.07	(0.04)	1.00
Al ₂ O ₃	0.09	(0.02)	0.05	(0.04)	0.16	(0.01)	0.24	(0.03)	0.16	(0.02)	0.04	(0.02)	0.45

Table A2. Cont.

Sample No	Type I												
	260		272-P4			272-P5		255-P2					
	Comment	Core	Rim	std	Core	Rim	std	Core	std	Core	std	Rim	
n	7	std	3	std	5	std	4	std	6	std	3	std	1
CaO	0.03	(0.01)	0.03	(0.02)	0.07	(0.01)	0.13	(0.04)	0.08	(0.02)	0.01	(0.00)	1.04
TiO ₂	0.29	(0.07)	0.28	(0.12)	0.48	(0.05)	0.33	(0.04)	0.47	(0.02)	0.10	(0.01)	0.09
Y ₂ O ₃	0.00	(0.01)	0.11	(0.11)	0.20	(0.26)	0.69	(0.60)	0.07	(0.12)	2.32	(1.31)	2.65
Nb ₂ O ₅	0.19	(0.05)	0.24	(0.04)	0.26	(0.03)	0.35	(0.06)	0.21	(0.04)	0.15	(0.01)	0.99
Ce ₂ O ₃	0.11	(0.05)	0.07	(0.03)	0.11	(0.03)	0.40	(0.04)	0.09	(0.03)	0.42	(0.28)	0.46
Nd ₂ O ₃	0.00	(0.00)	0.00	(0.00)	0.00	(0.00)	0.04	(0.04)	0.00	(0.00)	0.28	(0.01)	0.11
Gd ₂ O ₃	0.03	(0.03)	0.02	(0.02)	0.07	(0.05)	0.05	(0.02)	0.02	(0.01)	0.16	(0.11)	0.07
Dy ₂ O ₃	0.18	(0.04)	0.12	(0.03)	0.29	(0.04)	0.22	(0.02)	0.24	(0.05)	0.37	(0.11)	0.40
Ho ₂ O ₃	0.04	(0.04)	0.01	(0.01)	0.04	(0.05)	0.02	(0.03)	0.01	(0.03)	0.00	(0.00)	0.10
Er ₂ O ₃	0.04	(0.03)	0.06	(0.02)	0.06	(0.03)	0.12	(0.06)	0.05	(0.02)	0.47	(0.12)	0.79
Yb ₂ O ₃	0.03	(0.03)	0.04	(0.04)	0.07	(0.04)	0.09	(0.06)	0.03	(0.03)	1.41	(0.14)	2.14
UO ₂	0.07	(0.07)	0.11	(0.10)	0.16	(0.07)	0.04	(0.04)	0.08	(0.06)	0.22	(0.02)	0.36
ThO ₂	0.03	(0.04)	0.06	(0.05)	0.06	(0.02)	0.13	(0.07)	0.02	(0.02)	0.51	(0.23)	bdl
FeO	0.46	(0.36)	0.88	(1.03)	0.48	(0.06)	0.46	(0.06)	0.50	(0.02)	0.65	(0.38)	2.19
P ₂ O ₅	0.03	(0.03)	0.04	(0.03)	0.05	(0.03)	0.08	(0.07)	0.04	(0.02)	0.09	(0.05)	0.13
SnO ₂	0.26	(0.05)	0.36	(0.10)	0.78	(0.05)	0.65	(0.02)	0.82	(0.05)	0.17	(0.03)	bdl
Total	99.55		99.83		96.11		96.17		96.95		98.66		92.43
LREE ₂ O ₃	0.11	(0.05)	0.07	(0.03)	0.11	(0.03)	0.43	(0.03)	0.09	(0.03)	0.70	(0.27)	0.56
HREE ₂ O ₃	0.32	(0.03)	0.36	(0.10)	0.74	(0.33)	1.18	(0.73)	0.43	(0.14)	4.73	(1.51)	6.15
Structural formulae based on 4 oxygen atoms													
Si	1.030	(0.002)	1.020	(0.006)	1.025	(0.004)	1.020	(0.005)	1.027	(0.005)	1.014	(0.008)	0.937
Zr	0.930	(0.004)	0.933	(0.012)	0.913	(0.004)	0.910	(0.006)	0.918	(0.004)	0.898	(0.015)	0.887
Hf	0.014	(0.001)	0.013	(0.001)	0.013	(0.001)	0.012	(0.001)	0.012	(0.000)	0.010	(0.000)	0.010
Al	0.003	(0.001)	0.002	(0.002)	0.006	(0.000)	0.009	(0.001)	0.006	(0.001)	0.001	(0.001)	0.018
Ca	0.001	(0.000)	0.001	(0.001)	0.003	(0.000)	0.004	(0.001)	0.003	(0.001)	0.000	(0.000)	0.039
Ti	0.007	(0.002)	0.006	(0.003)	0.011	(0.001)	0.008	(0.001)	0.011	(0.001)	0.002	(0.000)	0.002
Y	0.000	(0.000)	0.002	(0.002)	0.003	(0.004)	0.012	(0.010)	0.001	(0.002)	0.039	(0.022)	0.049
Nb	0.003	(0.001)	0.003	(0.001)	0.004	(0.000)	0.005	(0.001)	0.003	(0.001)	0.002	(0.000)	0.015
Ce	0.001	(0.001)	0.001	(0.001)	0.001	(0.000)	0.005	(0.000)	0.001	(0.000)	0.005	(0.003)	0.006
Nd	0.000	(0.000)	0.000	(0.000)	0.000	(0.000)	0.000	(0.000)	0.000	(0.000)	0.003	(0.000)	0.001
Gd	0.000	(0.000)	0.000	(0.000)	0.001	(0.001)	0.000	(0.000)	0.000	(0.000)	0.002	(0.001)	0.001

Table A2. Cont.

Type I													
Sample No	260				272-P4				272-P5		255-P2		
Comment	Core	Rim		Core	Rim		Core	std	Core	std	Core	Rim	
n	7	std	3	std	5	std	4	std	6	std	3	std	1
Dy	0.002	(0.000)	0.001	(0.000)	0.003	(0.000)	0.002	(0.000)	0.002	(0.000)	0.004	(0.001)	0.004
Ho	0.000	(0.000)	0.000	(0.000)	0.000	(0.000)	0.000	(0.000)	0.000	(0.000)	0.000	(0.000)	0.001
Er	0.000	(0.000)	0.000	(0.000)	0.001	(0.000)	0.001	(0.001)	0.001	(0.000)	0.005	(0.001)	0.009
Yb	0.000	(0.000)	0.000	(0.000)	0.001	(0.000)	0.001	(0.001)	0.000	(0.000)	0.014	(0.001)	0.023
U	0.000	(0.001)	0.001	(0.001)	0.001	(0.000)	0.000	(0.000)	0.001	(0.000)	0.002	(0.000)	0.003
Th	0.000	(0.000)	0.000	(0.000)	0.000	(0.000)	0.001	(0.001)	0.000	(0.000)	0.004	(0.002)	0.000
Fe ²⁺	0.012	(0.009)	0.023	(0.027)	0.013	(0.002)	0.012	(0.001)	0.013	(0.000)	0.017	(0.010)	0.064
P	0.001	(0.001)	0.001	(0.001)	0.001	(0.001)	0.002	(0.002)	0.001	(0.001)	0.003	(0.001)	0.004
Sn	0.003	(0.001)	0.004	(0.001)	0.010	(0.001)	0.008	(0.000)	0.010	(0.001)	0.002	(0.000)	0.000
LREE	0.001	(0.001)	0.001	(0.00)	0.001	(0.00)	0.005	(0.00)	0.001	(0.00)	0.008	(0.00)	0.01
HREE	0.003	(0.000)	0.004	(0.00)	0.009	(0.01)	0.017	(0.01)	0.005	(0.00)	0.063	(0.02)	0.09

Type II														
Sample No	260-P23-1				261-P25-2					264-P22				
Comment	Core	Rim		Core	Rim Dark		Rim Bright		Core	Rim Dark				
n	3	std	3	std	4	std	5	std	3	std	5	std	5	std
SiO ₂	32.82	(0.08)	21.97	(0.35)	32.41	(0.08)	23.62	(1.57)	32.34	(0.92)	28.61	(2.92)	29.13	(3.85)
ZrO ₂	60.70	(0.21)	42.46	(0.74)	57.89	(0.29)	42.69	(3.10)	58.10	(0.36)	52.40	(4.32)	53.85	(4.84)
HfO ₂	1.18	(0.02)	0.84	(0.04)	0.88	(0.05)	0.68	(0.04)	1.08	(0.08)	0.92	(0.11)	1.00	(0.11)
Al ₂ O ₃	0.17	(0.03)	0.42	(0.12)	0.06	(0.03)	0.38	(0.07)	0.13	(0.03)	0.26	(0.21)	0.17	(0.23)
CaO	0.07	(0.02)	1.92	(0.42)	0.01	(0.01)	1.54	(0.38)	0.08	(0.07)	0.75	(0.54)	1.07	(0.93)
TiO ₂	0.28	(0.01)	0.06	(0.00)	0.09	(0.02)	0.21	(0.05)	0.13	(0.03)	0.08	(0.07)	0.10	(0.09)
Y ₂ O ₃	0.19	(0.02)	3.83	(0.48)	3.06	(0.07)	6.46	(0.64)	2.52	(0.34)	4.43	(0.97)	4.06	(0.95)
Nb ₂ O ₅	0.20	(0.01)	1.48	(0.35)	0.33	(0.04)	3.58	(0.66)	0.29	(0.18)	1.55	(1.21)	1.57	(1.80)
Ce ₂ O ₃	0.13	(0.01)	0.16	(0.03)	0.47	(0.09)	0.18	(0.06)	0.20	(0.12)	0.20	(0.07)	0.12	(0.06)
Nd ₂ O ₃	0.00	(0.00)	0.00	(0.00)	0.27	(0.04)	0.10	(0.05)	0.12	(0.03)	0.22	(0.12)	0.10	(0.01)
Gd ₂ O ₃	0.01	(0.00)	0.17	(0.04)	0.21	(0.03)	0.28	(0.05)	0.22	(0.04)	0.31	(0.04)	0.25	(0.06)
Dy ₂ O ₃	0.21	(0.00)	0.72	(0.05)	0.44	(0.01)	1.11	(0.14)	0.52	(0.16)	0.85	(0.24)	0.74	(0.19)
Ho ₂ O ₃	0.05	(0.05)	0.10	(0.10)	0.02	(0.02)	0.16	(0.04)	0.16	(0.07)	0.10	(0.08)	0.10	(0.08)
Er ₂ O ₃	0.14	(0.04)	0.66	(0.06)	0.51	(0.01)	1.08	(0.12)	0.52	(0.12)	0.76	(0.13)	0.80	(0.11)
Yb ₂ O ₃	0.36	(0.23)	1.10	(0.03)	0.86	(0.04)	1.15	(0.02)	0.60	(0.07)	1.35	(0.25)	1.73	(0.37)
UO ₂	0.16	(0.08)	0.21	(0.06)	0.26	(0.06)	0.08	(0.05)	0.15	(0.05)	0.35	(0.09)	0.31	(0.16)
ThO ₂	0.17	(0.08)	5.31	(0.58)	0.34	(0.25)	1.95	(0.50)	0.83	(0.34)	0.27	(0.16)	0.69	(0.57)

Table A2. Cont.

Sample No	Type II														
	260-P23-1				261-P25-2				264-P22						
	Comment	Core	Rim		Core	Rim Dark		Rim Bright		Core	Rim Dark				
n	3	std	3	std	4	std	5	std	3	std	5	std	5	std	
FeO	1.24	(0.68)	6.53	(1.59)	0.09	(0.02)	3.35	(0.74)	0.36	(0.14)	1.17	(0.93)	0.68	(0.90)	
P ₂ O ₅	0.06	(0.01)	0.34	(0.06)	0.10	(0.01)	0.33	(0.03)	0.11	(0.03)	0.23	(0.07)	0.25	(0.07)	
SnO ₂	0.48	(0.13)	0.03	(0.03)	0.02	(0.02)	0.05	(0.06)	0.05	(0.05)	0.06	(0.04)	0.03	(0.04)	
Total	98.60		88.32		98.32		88.97		98.52		94.87		96.74		
LREE ₂ O ₃	0.13	(0.01)	0.16	(0.03)	0.74	(0.08)	0.28	(0.09)	0.32	(0.16)	0.42	(0.18)	0.22	(0.07)	
HREE ₂ O ₃	0.94	(0.20)	6.59	(0.75)	5.09	(0.07)	10.24	(0.95)	4.54	(0.80)	7.80	(1.57)	7.68	(1.26)	
Structural formulae based on 4 oxygen atoms															
Si	1.019	(0.004)	0.848	(0.010)	1.023	(0.002)	0.878	(0.028)	1.019	(0.020)	0.958	(0.050)	0.956	(0.074)	
Zr	0.919	(0.005)	0.800	(0.011)	0.891	(0.002)	0.774	(0.030)	0.893	(0.004)	0.857	(0.029)	0.864	(0.028)	
Hf	0.011	(0.000)	0.009	(0.000)	0.008	(0.000)	0.007	(0.000)	0.010	(0.001)	0.009	(0.001)	0.009	(0.001)	
Al	0.006	(0.001)	0.019	(0.005)	0.002	(0.001)	0.017	(0.004)	0.005	(0.001)	0.011	(0.009)	0.007	(0.010)	
Ca	0.002	(0.001)	0.080	(0.018)	0.000	(0.000)	0.062	(0.017)	0.003	(0.003)	0.028	(0.020)	0.039	(0.036)	
Ti	0.007	(0.000)	0.002	(0.000)	0.002	(0.000)	0.006	(0.001)	0.003	(0.001)	0.002	(0.002)	0.003	(0.002)	
Y	0.003	(0.000)	0.079	(0.010)	0.051	(0.001)	0.128	(0.016)	0.042	(0.006)	0.080	(0.021)	0.072	(0.021)	
Nb	0.003	(0.000)	0.026	(0.006)	0.005	(0.000)	0.061	(0.013)	0.004	(0.003)	0.024	(0.019)	0.025	(0.029)	
Ce	0.002	(0.000)	0.002	(0.000)	0.005	(0.001)	0.002	(0.001)	0.002	(0.001)	0.002	(0.001)	0.001	(0.001)	
Nd	0.000	(0.000)	0.000	(0.000)	0.003	(0.000)	0.001	(0.001)	0.001	(0.000)	0.003	(0.001)	0.001	(0.000)	
Gd	0.000	(0.000)	0.002	(0.001)	0.002	(0.000)	0.004	(0.001)	0.002	(0.000)	0.003	(0.001)	0.003	(0.001)	
Dy	0.002	(0.000)	0.009	(0.001)	0.005	(0.000)	0.013	(0.002)	0.005	(0.002)	0.009	(0.003)	0.008	(0.003)	
Ho	0.000	(0.000)	0.001	(0.001)	0.000	(0.000)	0.002	(0.000)	0.002	(0.001)	0.001	(0.001)	0.001	(0.001)	
Er	0.001	(0.000)	0.008	(0.001)	0.005	(0.000)	0.013	(0.002)	0.005	(0.001)	0.008	(0.002)	0.008	(0.002)	
Yb	0.003	(0.002)	0.013	(0.000)	0.008	(0.000)	0.013	(0.001)	0.006	(0.001)	0.014	(0.003)	0.017	(0.004)	
U	0.001	(0.001)	0.002	(0.001)	0.002	(0.000)	0.001	(0.000)	0.001	(0.000)	0.003	(0.001)	0.002	(0.001)	
Th	0.001	(0.001)	0.047	(0.005)	0.002	(0.002)	0.017	(0.005)	0.006	(0.002)	0.002	(0.001)	0.005	(0.005)	
Fe ²⁺	0.032	(0.018)	0.211	(0.052)	0.002	(0.001)	0.105	(0.026)	0.009	(0.004)	0.034	(0.027)	0.020	(0.027)	
P	0.001	(0.000)	0.011	(0.002)	0.003	(0.000)	0.011	(0.001)	0.003	(0.001)	0.007	(0.002)	0.007	(0.002)	
Sn	0.006	(0.002)	0.000	(0.000)	0.000	(0.000)	0.001	(0.001)	0.001	(0.001)	0.001	(0.001)	0.000	(0.000)	
LREE	0.002	(0.00)	0.002	(0.00)	0.008	(0.00)	0.004	(0.00)	0.004	(0.00)	0.005	(0.00)	0.003	(0.00)	
HREE	0.010	(0.00)	0.112	(0.01)	0.071	(0.00)	0.173	(0.02)	0.063	(0.01)	0.116	(0.03)	0.110	(0.03)	

Table A2. Cont.

Sample No	Type II								Type III			
	266-P3-3c				270-P8-1				265-15-1		261-25	
	Comment	Core	Rim		Core	Rim			Core	Rim	Core	
n	4	std	5	std	4	std	4	std	1	1	7	std
SiO ₂	32.41	(0.25)	31.81	(0.39)	31.01	(0.34)	30.98	(0.27)	33.20	30.29	33.32	(0.19)
ZrO ₂	59.71	(0.39)	58.22	(0.89)	56.27	(0.72)	56.84	(0.30)	61.93	58.77	60.60	(0.49)
HfO ₂	1.21	(0.05)	1.09	(0.07)	1.88	(1.03)	1.49	(0.56)	3.12	3.08	1.24	(0.04)
Al ₂ O ₃	0.15	(0.02)	0.03	(0.04)	0.11	(0.10)	0.07	(0.09)	0.29	0.27	0.15	(0.03)
CaO	0.06	(0.03)	0.02	(0.01)	0.03	(0.01)	0.01	(0.01)			0.04	(0.01)
TiO ₂	0.09	(0.03)	0.04	(0.02)	0.12	(0.05)	0.11	(0.02)			0.21	(0.04)
Y ₂ O ₃	0.53	(0.09)	3.09	(0.88)	4.27	(1.24)	4.11	(0.45)	0.90	0.84	1.51	(0.25)
Nb ₂ O ₅	0.24	(0.03)	0.29	(0.06)	0.56	(0.09)	0.72	(0.15)			0.12	(0.02)
Ce ₂ O ₃	0.26	(0.05)	0.12	(0.17)	0.05	(0.04)	0.06	(0.03)			0.32	(0.17)
Nd ₂ O ₃	0.00	(0.00)	0.10	(0.09)	0.08	(0.07)	0.18	(0.03)			0.08	(0.09)
Gd ₂ O ₃	0.02	(0.01)	0.19	(0.08)	0.52	(0.18)	0.44	(0.06)			0.07	(0.03)
Dy ₂ O ₃	0.13	(0.04)	0.62	(0.20)	0.54	(0.18)	0.52	(0.05)			0.23	(0.04)
Ho ₂ O ₃	0.02	(0.03)	0.09	(0.06)	0.10	(0.05)	0.05	(0.06)			0.08	(0.06)
Er ₂ O ₃	0.23	(0.05)	0.74	(0.24)	0.40	(0.02)	0.51	(0.13)			0.27	(0.05)
Yb ₂ O ₃	0.85	(0.06)	1.21	(0.21)	0.55	(0.12)	0.68	(0.15)			0.58	(0.07)
UO ₂	0.13	(0.06)	0.09	(0.02)	0.16	(0.07)	0.06	(0.04)			0.02	(0.03)
ThO ₂	0.08	(0.05)	0.59	(0.35)	0.09	(0.03)	0.03	(0.04)			0.06	(0.05)
FeO	0.54	(0.42)	0.18	(0.08)	0.15	(0.09)	0.16	(0.13)	bdl	bdl	0.20	(0.04)
P ₂ O ₅	0.09	(0.04)	0.17	(0.06)	0.15	(0.06)	0.13	(0.02)			0.06	(0.03)
SnO ₂	0.22	(0.04)	0.06	(0.06)	0.10	(0.10)	0.07	(0.06)			0.01	(0.01)
Total	96.94		98.74		97.15		97.21		99.87	93.60	99.15	
LREE ₂ O ₃	0.26	(0.05)	0.22	(0.25)	0.13	(0.10)	0.23	(0.06)	0.00	0.00	0.41	(0.25)
HREE ₂ O ₃	1.78	(0.13)	5.94	(1.61)	6.38	(1.71)	6.31	(0.80)	0.90	0.84	2.74	(0.33)
Structural formulae based on 4 oxygen atoms												
Si	1.025	(0.007)	1.008	(0.005)	0.999	(0.005)	0.997	(0.009)	1.020	1.000	1.025	(0.002)
Zr	0.921	(0.004)	0.899	(0.013)	0.884	(0.005)	0.892	(0.005)	0.955	0.975	0.910	(0.003)
Hf	0.011	(0.000)	0.010	(0.001)	0.017	(0.009)	0.014	(0.005)	0.011	0.010	0.011	(0.000)
Al	0.006	(0.001)	0.001	(0.002)	0.004	(0.004)	0.003	(0.003)	0.007	0.010	0.005	(0.001)
Ca	0.002	(0.001)	0.001	(0.000)	0.001	(0.001)	0.000	(0.000)			0.001	(0.000)
Ti	0.002	(0.001)	0.001	(0.000)	0.003	(0.001)	0.003	(0.001)			0.005	(0.001)
Y	0.009	(0.002)	0.052	(0.015)	0.073	(0.022)	0.070	(0.008)	0.015	0.015	0.025	(0.004)
Nb	0.003	(0.000)	0.004	(0.001)	0.008	(0.001)	0.010	(0.002)			0.002	(0.000)
Ce	0.003	(0.001)	0.001	(0.002)	0.001	(0.000)	0.001	(0.000)			0.004	(0.002)
Nd	0.000	(0.000)	0.001	(0.001)	0.001	(0.001)	0.002	(0.000)			0.001	(0.001)
Gd	0.000	(0.000)	0.002	(0.001)	0.006	(0.002)	0.005	(0.001)			0.001	(0.000)

Table A2. Cont.

Sample No	Type II								Type III			
	266-P3-3c				270-P8-1				265-15-1		261-25	
	Comment	Core	Rim	std	Core	Rim	std	Core	Rim	Core	std	
n	4	5	std	4	4	std	1	1	7	std		
Dy	0.001	(0.000)	0.006	(0.002)	0.006	(0.002)	0.005	(0.000)			0.002	(0.000)
Ho	0.000	(0.000)	0.001	(0.001)	0.001	(0.001)	0.001	(0.001)			0.001	(0.001)
Er	0.002	(0.001)	0.007	(0.002)	0.004	(0.000)	0.005	(0.001)			0.003	(0.000)
Yb	0.008	(0.001)	0.012	(0.002)	0.005	(0.001)	0.007	(0.001)			0.006	(0.000)
U	0.001	(0.000)	0.001	(0.000)	0.001	(0.000)	0.000	(0.000)			0.000	(0.000)
Th	0.001	(0.000)	0.004	(0.003)	0.001	(0.000)	0.000	(0.000)			0.001	(0.000)
Fe ²⁺	0.014	(0.011)	0.005	(0.002)	0.004	(0.002)	0.004	(0.003)			0.005	(0.001)
P	0.002	(0.001)	0.005	(0.002)	0.004	(0.002)	0.003	(0.000)			0.001	(0.001)
Sn	0.003	(0.001)	0.001	(0.001)	0.001	(0.001)	0.001	(0.001)			0.000	(0.000)
LREE	0.003	(0.001)	0.003	(0.003)	0.002	(0.001)	0.003	(0.001)			0.005	(0.003)
HREE	0.021	(0.002)	0.080	(0.022)	0.095	(0.027)	0.093	(0.011)			0.036	(0.005)

std*: standard deviation; bdl*: below detectable level.

References

1. Eby, N.G. The A-type granitoids: A review of their occurrence and chemical characteristics and speculations on their petrogenesis. *Lithos* **1990**, *26*, 115–134. [[CrossRef](#)]
2. Salvi, S.; Williams-Jones, A.E. The role of hydrothermal processes in concentrating high-field strength elements in the Strange Lake peralkaline complex, northeastern Canada. *Geochim. Cosmochim. Acta* **1996**, *60*, 1917–1932. [[CrossRef](#)]
3. Dostal, J.; Kontak, D.J.; Karl, S.M. The Early Jurassic Bokan Mountain peralkaline granitic complex (southeastern Alaska): Geochemistry, petrogenesis and rare-metal mineralization. *Lithos* **2014**, *202–203*, 395–412. [[CrossRef](#)]
4. Harris, N.B.W.; Marriner, G.F. Geochemistry and petrogenesis of a peralkaline granite complex from the Midian Mountains, Saudi Arabia. *Lithos* **1980**, *13*, 325–337. [[CrossRef](#)]
5. Kovalenko, V.I.; Tsaryeva, G.M.; Goreglyad, A.V.; Yarmolyuk, V.V.; Troitsky, V.A. The peralkaline granite-related Khaldzan-Buregtey rare metal (Zr, Nb, REE) deposit, Western Mongolia. *Econ. Geol.* **1995**, *90*, 530–547. [[CrossRef](#)]
6. Birket, T.C.; Miller, R.R. Comment on the role of hydrothermal processes in the granite-hosted Zr, Y, REE deposit at Strange Lake, Quebec/Labrador: Evidence from fluid inclusion. *Geochem. Cosmochim. Acta* **1991**, *55*, 3443–3445. [[CrossRef](#)]
7. Boily, M.; Williams-Jones, A.E. The role of magmatic and hydrothermal processes in the chemical evolution of the Strange Lake plutonic complex, Quebec/Labrador. *Contrib. Mineral. Petrol.* **1994**, *118*, 33–47. [[CrossRef](#)]
8. Salvi, S.; Williams-Jones, A.E. The role of hydrothermal processes in the granite-hosted Zr, Y, REE deposit at Strange Lake, Quebec/Labrador: Evidence from fluid inclusions. *Geochim. Cosmochim. Acta* **1990**, *54*, 2403–2418. [[CrossRef](#)]
9. Kempe, U.; Gotze, J.; Dandar, S.; Habermann, D. Magmatic and metasomatic processes during formation of the Nb–Zr–REE deposits Khaldzan Buregte and Tsakhir (Mongolian Altai): Indications from a combined CL-SEM study. *Mineral. Mag.* **1999**, *63*, 165–177. [[CrossRef](#)]
10. Kempe, U.; Möckel, R.; Graupner, T.; Kynicky, J.; Dombon, E. The genesis of Zr–Nb–REE mineralization at Khaldzan Buregte (Western Mongolia) reconsidered. *Ore Geol. Rev.* **2015**, *64*, 602–625. [[CrossRef](#)]
11. Kovalenko, V.I.; Yarmolyuk, V.V.; Sal'nikova, E.B.; Kartashov, P.M.; Kovach, V.P.; Kozakov, I.K.; Kozlovskij, A.M.; Kotov, A.B.; Ponomarchuk, V.A.; Listratova, E.N.; et al. The Khaldzan Buregtei massif of peralkaline rare-metal igneous rocks: Structure, geochronology, and geodynamic setting in the Caledonides of western Mongolia. *Petrology* **2004**, *12*, 467–494.
12. Miranov, U.B.; Minin, A.D. *Report on Western Mongolia, Altai-Hohiy Ridge Geological Mapping at Scale 1:50000*; Unpublished Report; Mongolian Geological Central Fond: Ulaanbaatar, Mongolia, 1991; Report 4505.
13. Yarmolyuk, V.V.; Kuzmin, M.I.; Ernst, R.E. Interplate geodynamics and magmatism in the evolution of the Central Asian Orogenic Belt. *J. Asian Earth Sci.* **2014**, *93*, 158–179. [[CrossRef](#)]
14. Watanabe, Y.; Sanematsu, K. *Khaldzan Burgedtei Rare Earth Project Progress Report No. 2: Report on Field Survey*; Exploration Work Report; Mongolian Lantanoide Corporation: Ulaanbaatar, Mongolia, 2011.
15. Corfu, F.; Hancher, J.M.; Hoskin, P.W.O.; Kinny, P. Atlas of zircon textures. *Rev. Mineral. Geochem.* **2003**, *53*, 469–500. [[CrossRef](#)]
16. Linnen, R.; Keppler, H. Melt composition control of Zr/Hf fractionation in magmatic processes. *Geochim. Cosmochim. Acta* **2002**, *66*, 3293–3301. [[CrossRef](#)]
17. Fernando, B.; Pilar, M.; Miguel, O.T. A LA-ICP-MS evaluation of Zr reservoirs in common crystal rocks: Implications for Zr and Hf geochemistry, and zircon-forming processes. *Can. Mineral.* **2006**, *44*, 693–714.
18. Forester, H.J.; Tischendorf, G.; Trumbull, R.B.; Gottesmann, B. Late-Collisional Granites in the Variscan Erzgebirge, Germany. *J. Petrol.* **1999**, *40*, 1613–1645. [[CrossRef](#)]
19. Hoshino, M.; Watanabe, Y.; Murakami, H.; Kon, Y.; Tsunematsu, M. Formation process of zircon associated with REE-Fluorocarbonate and Niobium minerals in the Nechalacho REE deposit, Thor Lake, Canada. *Resour. Geol.* **2012**, *63*, 1–26. [[CrossRef](#)]
20. Rodney, C.E.; Alkiviathes, M.; Lumin, W. Radiation effects in zircon. *Mineral. Geochem.* **2003**, *53*, 387–420.

